FIU Electronic Theses and Dissertations | University Graduate School

3-31-2017

Nano-Confined Metal Oxide in Carbon Nanotube Composite Electrodes for Lithium Ion Batteries

Alexandra J. Henriques
Florida International University, ahenr014@fiu.edu

FLORIDA INTERNATIONAL UNIVERSITY

Miami, Florida

NANO-CONFINED METAL OXIDE IN CARBON NANOTUBE COMPOSITE

ELECTRODES FOR LITHIUM ION BATTERIES

A thesis submitted in partial fulfillment of

the requirements for the degree of

MASTER OF SCIENCE

in

MATERIALS SCIENCE AND ENGINEERING

by

Alexandra J. Henriques

2017

To: Interim Dean Ranu Jung
    College of Engineering and Computing

This thesis, written by Alexandra J. Henriques, and entitled Nano-Confined Metal Oxide In Carbon Nanotube Composite Electrodes For Lithium Ion Batteries, having been approved in respect to style and intellectual content, is referred to you for judgment.

We have read this thesis and recommend that it be approved.

_____
Zhe Cheng

_____
Norman Munroe

_____
Chunlei Wang, Major Professor

Date of Defense: March 31, 2017

The thesis of Alexandra J. Henriques is approved.

_____
Interim Dean Ranu Jung
College of Engineering and Computing

_____
Andrés G. Gil
Vice President for Research and Economic Development
and Dean of the University Graduate School

Florida International University, 2017

ABSTRACT OF THE THESIS

NANO-CONFINED METAL OXIDE IN CARBON NANOTUBE COMPOSITE

ELECTRODES FOR LITHIUM ION BATTERIES

by

Alexandra J. Henriques

Florida International University, 2017

Miami, Florida

Professor Chunlei Wang, Major Professor

Lithium ion batteries (LIB) are one of the most commercially significant secondary batteries, but in order to continue improving the devices that rely on this form of energy storage, it is necessary to optimize their components. One common problem with anode materials that hinders their performance is volumetric expansion during cycling. One of the methods studied to resolve this issue is the confinement of metal oxides with the interest of improving the longevity of their performance with cycling. Confinement of metal oxide nanoparticles within carbon nanotubes has shown to improve the performance of these anode materials versus unconfined metal oxides. Here, electrostatic spray deposition (ESD) is used to create thin films of nano-confined tin oxide/CNT composite as the active anode material for subsequent property testing of assembled LIBs. This thesis gives the details of the techniques used to produce the desired anode materials and their electrochemical characterization as LIB anodes.

TABLE OF CONTENTS

LIST OF FIGURES

ABBREVIATIONS AND ACRONYMS

CNT   Carbon nanotube

CV   Cyclic voltammetry

CVD   Chemical vapor deposition

EDS   Energy dispersive spectroscopy

EIS   Electrochemical impedance spectroscopy

ESD   Electrostatic spray deposition

FESEM   Field-emission scanning electron microscope

HRTEM   High-resolution transmission electron microscopy

LIB   Lithium ion battery

MWCNT   Multi-walled carbon nanotube

RGO   Reduced graphene oxide

SEM   Scanning electron microscopy

TEM   Transmission electron microscopy

XRD   X-ray diffraction

CHAPTER I

INTRODUCTION

The key objective of this master's thesis project was to create and test thin films of a lithium ion battery (LIB) anode active composite material made of tin oxide (SnO_2) and carbon nanotubes (CNTs). The chosen thin film deposition method was electrostatic spray deposition (ESD). This composite active material was specifically chosen to create a nanostructure with tin oxide nanoparticles confined within the inner channels of the carbon nanotubes with the goal of improving electrochemical performance. The composite material was characterized using x-ray diffraction (XRD), scanning electron microscopy (SEM), and transmission electron microscopy (TEM). Electrochemical studies were carried out via cyclic voltammetry (CV), galvanostatic discharge-charge testing, rate capability testing, and electrochemical impedance spectroscopy (EIS). Electrochemical testing was used to determine the specific capacity of the active anode material of interest as well as the extent of retention of capacity with cell cycling. The research results show that the nano-confined SnO_2-in-CNT composite materials are promising anodes for use in LIBs. Furthermore, the weight ratio of SnO_2 to CNT that showed the best performance was 20:80.

1.1 Motivation

The development of high capacity rechargeable lithium-ion batteries (LIBs) is crucial given the insatiable energy demands that come with the rapidly developing technological landscape that exists in modern society. From portable technologies and medical equipment to alternative energy sources, the continual improvement of batteries

and fuel cells has been rendered invaluable for society to continue improving. With the demand for renewable energy and electric vehicles, improved energy storage technology is necessary to enable an effective transition to more environmentally sound practices and energy infrastructure.[1,2]
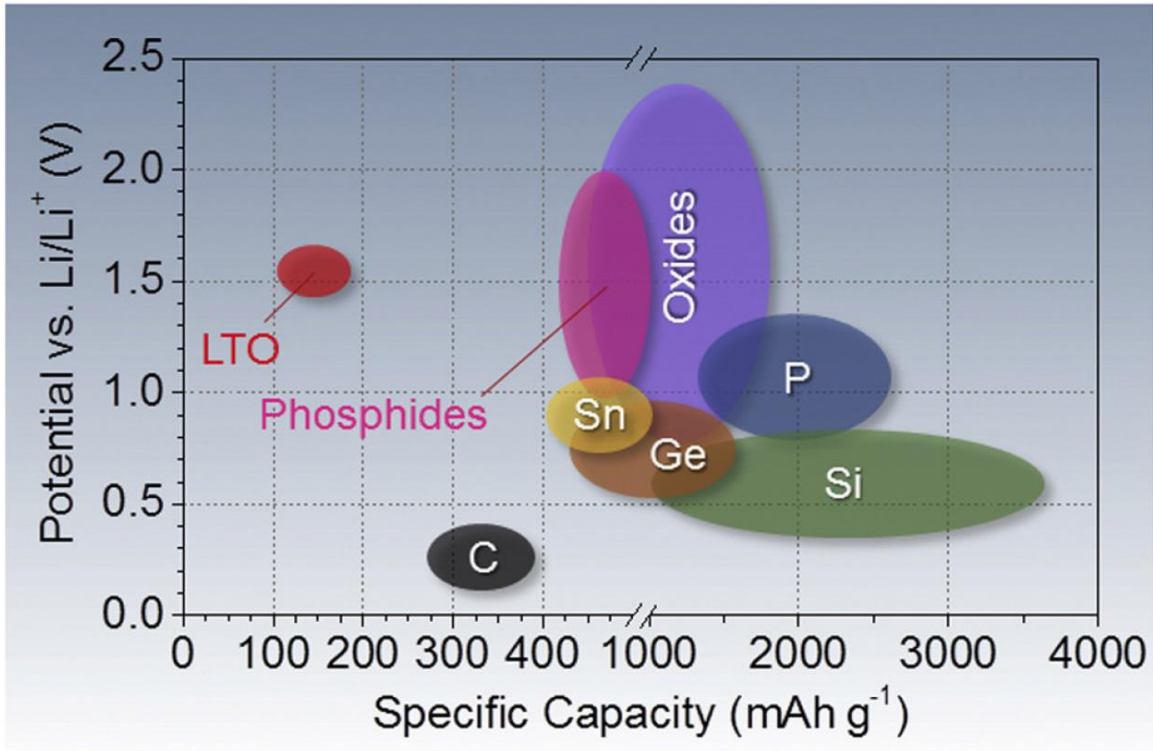
Figure 1: Specific capacities and potential vs. Li/Li+ for various anode materials[3]

1.1.1 Metal Oxides as Anode Materials

One of the major areas of research focus is the development of high performance advanced electrochemical materials for the electrodes of LIBs. Deviating from typical intercalation anodes such as graphite, metal oxides (M_xO_y) with conversion and/or alloying reaction mechanisms have become one of the areas of research focus in recent years because of their high theoretical capacities as active anode materials.[1] Figure 1 shows the

specific capacities and potentials vs. lithium of various anode materials that have been explored. Carbon, which is presently a widely commercially used anode material, has a relatively low specific capacity, where as metallic tin and metal oxides, including tin oxide (SnO_2), have higher specific capacities. In this research, SnO_2 was chosen as the metal oxide of interest because its theoretical capacity is more than twice that of the current anode of choice, graphite, with a theoretical capacity of ~790 mAh/g for SnO_2 versus ~372 mAh/g for graphite.[2,4,5] Additionally, anodes made with SnO_2 active materials can be paired with a large variety of cathode materials because these anodes can work at a relatively low potential, similar to graphite and the material is inexpensive and nontoxic.[4,5] The main drawbacks of the use of most metal oxides as an anode material in LIBs is their low electrical conductivity and their large volume change during cell cycling, which is true of SnO_2 as well.[1,2,4] Volumetric expansion of the anode material is associated with cracking, particle shuffling, and pulverization of the active material as well as its delamination from the current collector.[1] Thus, a variety of solutions to these issues are being explored to better leverage the possible benefits of metal oxide anode materials.

1.1.2 Nanostructure and Carbon Matrix

One of the methods considered to solve the issue of the volumetric expansion during the cycling of cells with metal oxide-based anodes is the nanostructuring of the active material.[1,2,4,6,7] Nanostructured anode materials offer the advantage of a greater surface area to volume ratio versus bulk or larger particulate materials.[2] This allows for room to accommodate volume change, reducing the issues that typically cause capacity fading and eventual failure.[2] A carbon matrix, such as a carbon nanotube-based matrix, is

of interest given its improved electrical conductivity versus metal oxides and its good mechanical strength.[8]

1.2 Research objectives

The overall goal of this project was to synthesize a LIB anode material that confined tin oxide within a CNT structure and test it electrochemically. The secondary goals included:

(1) Testing of various weight ratios of SnO_2 to CNTs in the composite active material to determine best electrochemical performance,

(2) Optimization of ESD parameters to create a porous thin film of the active material,

(3) Comparison of the electrochemical performance of the target material with control groups to validate the results, and

(4) Evaluation of material structure characteristics via SEM, TEM, and XRD to determine structure effects on electrochemistry.

The research hypothesis was that the creation of a thin film of tin oxide nanoparticles confined within CNTs via ESD will improve the performance of the tin oxide active material as a LIB anode by increasing interfacial charge storage, limiting its volumetric expansion, improving electrical conductivity, reducing byproduct aggregation, and buffering stresses generated during battery cycling.

The second chapter will present the relevant background information about LIB anode materials and the chemistry involved during the cycling of LIBs with carbon and tin oxide anodes as well as information about the chosen microstructure/nanostructure of the active anode material. Chapter three details the experimental methods used to create the

4

active anode material of interest, assemble cells containing this material, electrochemical testing carried out on these cells, and additional characterization of the materials. Chapter four gives the results of the electrochemical testing and material characterization that was done and chapter five elucidates the conclusions drawn from the results obtained.

CHAPTER II

LITERATURE REVIEW

This chapter contains a review of the relevant literature pertaining to rechargeable battery technology, lithium ion batteries, anode materials common in LIBs, and studies conducted on materials used for electrochemical storage with similarities in nanostructure or composition to the work presented in the subsequent chapters.

2.1 Rechargeable Batteries and Lithium Ion Batteries

Batteries are typically categorized as either primary or secondary based on their ability to be recharged.[2] Primary batteries are those that are only used once and cannot be recharged.[2] Secondary batteries, also called rechargeable batteries, are those that operate via a reversible chemical reaction that allows them to be discharged and recharged for repeated use.[2] The four main types of rechargeable battery are lead-acid, such as those used in traditional vehicles, Ni-Cd, Ni-MH, and LIBs.[2] Presently, one of the most commercially significant and widely used secondary batteries is the LIB.[2] Figure 2 shows a comparison of the energy densities of the various common rechargeable batteries. From this plot it is evident that the higher gravimetric energy density and volumetric energy density associated with LIBs is a main factor in their commercial use. Additionally, LIBs generally tend to have a reasonably high cycle life (>1,000 cycles), making them an advantageous choice.[2]
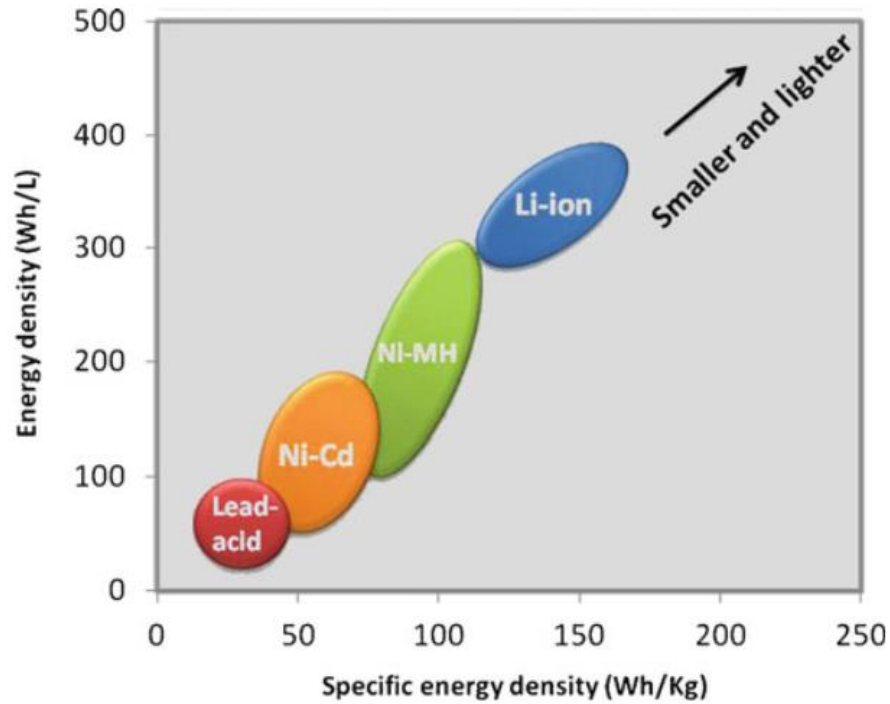
Figure 2: Comparison of energy densities of various secondary batteries.[2]

2.2 Metal Oxides as Anode Materials

Metal oxides (M_xO_y) have become an area of research focus in recent years because of their high theoretical capacities as active anode materials. Table 1 shows a comparison of the theoretical capacities of some materials of interest both in the present work and the literature.

Table 1: Selected theoretical specific capacities

Metal Oxide or Metal	Theoretical Specific Capacity (mAh/g)
MnO_2	1,233 [2]
MnO	756 [2]
NiO	718 [2]
Sn	993 [2]
SnO_2	783 [2]

Currently, the most widely used anode is made of graphitic carbon. The theoretical capacity reported for carbon is relatively low, about 372 mAh/g.[2,9] It is the standard, however, because of its stability as an anode, as it tends to retain its capacity for the lifetime of the battery.[2,9] Some of the metal oxides of interest in this work, including MnO_2 and SnO_2 have theoretical capacities of 1,233 and 783 mAh/g respectively.[2] The improvement in theoretical capacity, though promising, does not translate directly to a better LIB with use of the pure, bulk oxide material as the active component of a LIB anode, however. This is a result not only of their poor electrical conductivities, but also of the volumetric change that occurs in these materials during their reaction processes with lithium. In the case of SnO_2, an expansion of the material during cycling of about 260% is observed.[2] Such volumetric change can cause cracking and pulverization of the anode material, loss of contact with the current collector, and eventual failure of the LIB. The reactions for the two aforementioned materials of interest are shown in Equations 1-3.

$$SnO_2 + 4\ Li+ + 4\ e^- \rightarrow Sn + 2\ Li_2O \qquad\qquad [1]$$

$$Sn + x\ Li^+ + x\ e^- \leftrightarrow Li_xSn\ (0 \leq x \leq 4.4) \qquad\qquad [2]$$

$$MnO_2 + 4\ Li^+ + 4\ e^- \leftrightarrow Mn + 2\ Li_2O \qquad\qquad [3]$$
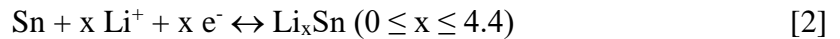
SnO_2 undergoes a two-step alloying reaction with lithium to form metallic tin as an intermediate species. Equation 1, for SnO_2 is associated with a theoretical specific capacity of 711 mAh/g, and is followed by the reversible reaction listed as Equation 2, which has a theoretical capacity of 993 mAh/g, leading to an overall theoretical capacity of 783 mAh/g for SnO_2. During the first reaction step, SnO_2 reacts with lithium to form metallic tin and Li_2O, which is also beneficial to the performance of SnO_2 based electrode materials relative to Sn metal.[2] This is caused by the buffering matrix formed by the Li_2O that prevents the

aggregation of Sn during cycling, which tends to happen in pure tin electrodes.[2] MnO_2, like many transition metal oxides, undergoes a conversion reaction with lithium, as written in Equation 3.

In the traditional literature, with bulk SnO_2, the first reaction shown as equation 1 was typically regarded as irreversible.[10] More recent work, however, has shown that nanoparticulate SnO_2 can exhibit some reversibility of the first conversion reaction step leading to an extension of the theoretical capacity to as much as 1490 $mAhg^{-1}$.[10]

2.3 Nanostructural Confinement of Metal Oxides in Carbon

Given the promising theoretical capacities of metal oxides and metals for use as anode materials in LIBs,[2] it is particularly of interest to find a way to mitigate the issues encountered when using these materials in anodes. One method of doing so that has been explored and proven promising is nanostructuring of the materials in question.[2,9,11–14] The nanostructuring of these materials not only has been shown to improve their resistance to failure due to volumetric change, but also have better performance because of their high surface area to volume ratio.[2]

In addition to nanostructuring the metal oxides, an additional approach to further improving the performance of the materials is by confining these nanostructures within a matrix.[15–17] The chosen materials that show the most promise are carbon based because graphitic sp^2 hybridized carbon, as in graphene and carbon nanotubes (CNTs), has excellent electrical conductivity and mechanical properties.[8] Agrawal *et al.* showed that CNTs, specifically, have a significant damping effect, which is of interest to buffer the

stresses generated due to volumetric change in the metal oxide nanoparticles during reaction with lithium ions in the LIB.[8]

2.3.1 Sn@Carbon Nanoparticles in Bamboo-like Hollow Carbon Nanofibers

Yu *et al.* explored the use of a carbon structure to confine Sn@carbon nanoparticles for use as a LIB anode.[16] In this study, the Sn@carbon particles were encapsulated within hollow carbon nanofibers (CNFs) via electrospinning and pyrolysis to address the issues of volume change and tin particle agglomeration.[16] Figure 3 shows the TEM images confirming the encapsulation of the Sn@carbon particles within hollow CNFs.[16]
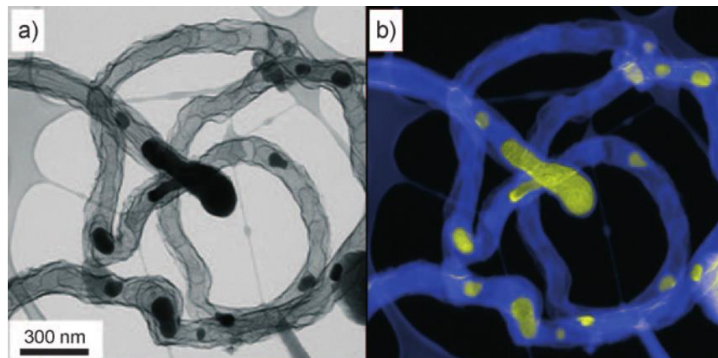
Figure 3: (a) Bright field (BF) zero-loss filtered elastic TEM image of CNFs with Sn@carbon nanoparticles and (b) Elemental mapping confirming the tin and carbon content in the predicted locations.[16]

In this study, it was shown that the composite material for the anode exhibited a reversible capacity, after cycling assembled cells 200 times at 5 C, of 737 mAh/g.[16] Figure 4 shows the representative cyclic voltammograms (CV) taken with a scan speed of 0.2 mV/s and the electrochemical performance for electrode cycled between 0.01 and 3 V vs. Li^+/Li with comparison to commercially available nanoscale tin.
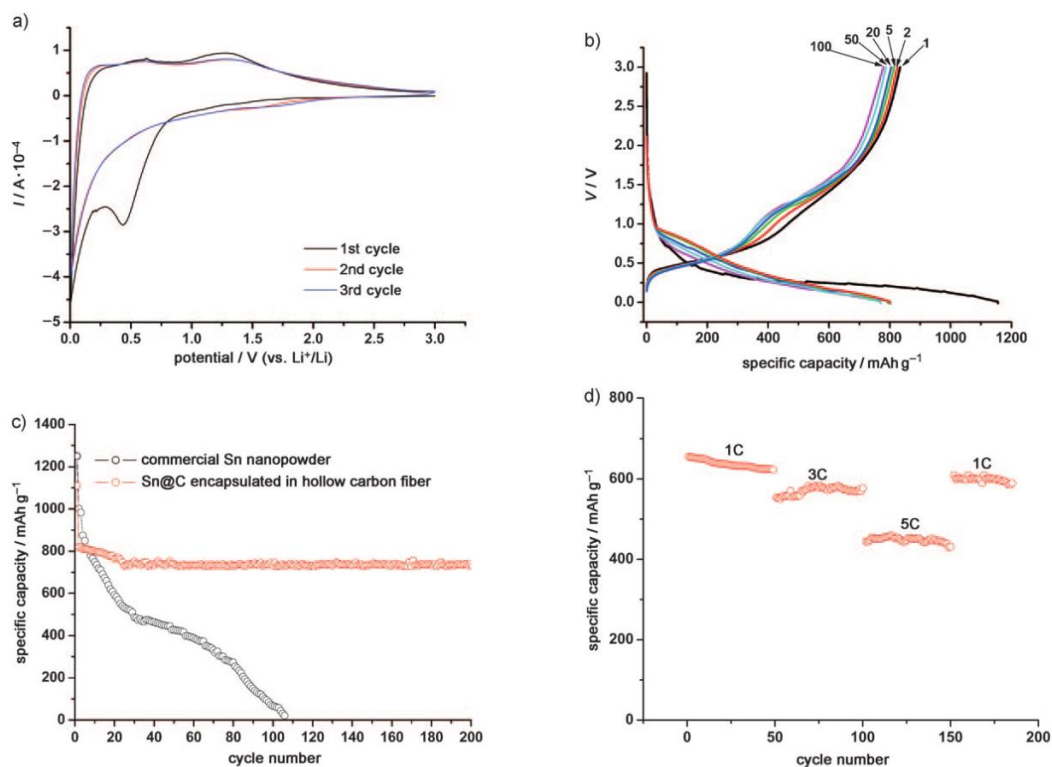
Figure 4: (a) CV for Sn@carbon encapsulated in CNFs with scan speed of 0.2 mV/s (b-d) Electrochemical performance vs. Li$^+$/Li with cycling between 0.01 and 3 V.[16]

2.3.2 Comparison of SnO$_2$ Based Anodes with Various Nanostructured Carbons

Guo *et al*. conducted work on monodisperse SnO$_2$ particles on reduced graphene oxide (RGO) platelets and compared these results with those of a variety of tin oxide and carbon structured anode material work.[10] Table 2 shows a summary of the work compared by Guo *et al.* in their review, indicating the current rates at which various studies tested their materials of interest, the observed discharge capacities reported, and their retention of capacity with cycling (indicating number of cycles used).[10] From the work presented by Guo *et al.*, the monodisperse SnO$_2$ on RGO had the best discharge specific capacity of 1057 mAh/g in the second cycle and best capacity retention of 1036 mAh/g after 400 cycles when tested at a current rate of 500 mAh/g.

Table 2: Comparison of various SnO₂ and carbon composite electrode capacities for LIB anodes

Sample	Current Rate (mA/g)	Discharge Capacity (mAh/g)	Capacity Retention (mAh/g)/(cycles)
Monodisperse SnO₂ on RGO	500	1057 (2nd cycle)	1036/400
SnO₂/Graphene	100	931	718/200
SnO₂ *nanosheets*	156	762	534/50
SnO₂/Graphene	50	1080	649/30
SnO₂/CNF	100		383/30
SnO₂/CNT	200		497/300

2.3.3 Nanoconfined MnO₂ in CNTs

Interest in the nanoconfinement of metal oxides in carbon channels stems largely from the work of Chmiola *et al.* who used a carbon structure into which nanometer-scale pores were etched and subsequently filled with MnO₂ particles.[18] This work assessed the capacitance of such materials and found that gaps between the carbon structure and metal oxide particle smaller than 1.5 nm can contribute to charge storage far more than was previously thought.[18] This improved charge storage is thought to stem from a pseudocapacitive effect, which could, in turn, be observed with confinement of particles in the inner channels of carbon nanotubes.

The groundwork and proof-of-concept for the encapsulation of particulate metal oxides within carbon nanotubes, specifically, came from the work of Chen *et al.* in the nanoconfinement of MnO₂ nanoparticles within CNTs for use in a capacitor application.[15] In this work, a reliable method was devised for the confinement of manganese dioxide nanoparticles within multiwalled (MW) CNTs and an improvement was shown for the material of interest, which contained the nanoparticles within the CNTs versus the particles outside CNTs, just the CNTs, or just the MnO₂.[15] Figure 5 shows the TEM micrographs

indicating the presence of the MnO_2 particles within the CNTs as well as the comparison with the samples made that had MnO_2 outside the CNTs.[15]
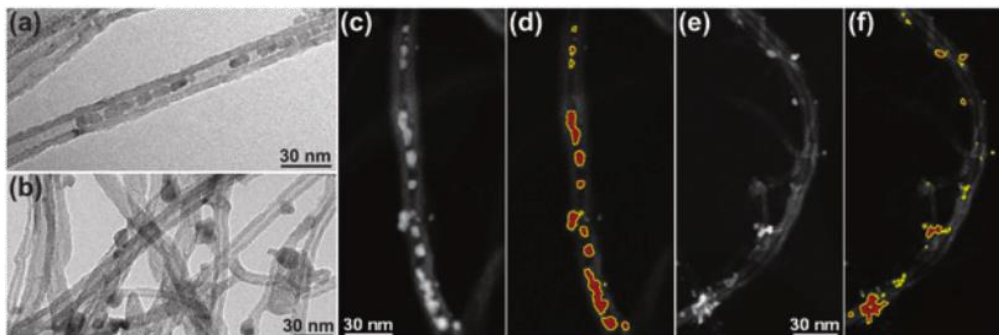
Figure 5: (a) BF TEM micrograph of MnO_2 confined within CNT, (b) MnO_2 outside CNT, (c-f) High angle area diffraction images and elemental analysis showing confinement of MnO_2 within CNTs.[15]

The study showed improved reversibility and capacity of the composite material created in this study.[15] Additionally, the procedure developed was able to reliably achieve up to 20% mass loading of the MnO_2 nanoparticles within the MW CNTs.[15] Figure 6 shows the comparison of the specific capacitance of the various samples tested, cyclic voltammetry, and tabulated data.[15] From these results, it was found that the MnO_2 confined within the CNTs gave a specific capacitance as high as 225 F/g and when normalized by MnO_2 gave a specific capacitance of 1250 F/g.[15]

In this study, electrostatic spray deposition (ESD) was used to form a thin film of the electrode materials of interest on a substrate that was used as the current collector for subsequent testing of the electrochemical performance of these anodes.[15] This technique is of interest for use because of its versatility for film deposition of many different materials and morphologies, as well as its ability to allow for simultaneous heat treatment, if needed, up to moderate temperatures.[9,15,19–21]

a)

b)

c)

d)

Sample	Specific capacitance obtained by CV curves (F g^{-1})[a]	Specific capacitance normalized by MnO$_2$ (F g^{-1})
cCNTs	25	–
oCNTs	37	–
MnO$_2$	13	13
MnO$_2$-out-CNT	144	790[b]
MnO$_2$-in-CNT	225	1250[c]

[a] Calculated by integrating area of CV curves. [b] Based on weight percentage of MnO$_2$ by subtracting the specific capacitance of blank cCNTs. [c] Based on weight percentage of MnO$_2$ by subtracting the specific capacitance of blank oCNTs.

Figure 6: (a) Specific capacitance comparison, (b) comparison of normalized specific capacitance between MnO$_2$ outside vs. inside CNTs for composite anodes, (c) CV comparing CNTs without MnO$_2$ to CNTs with MnO$_2$ both outside and inside, (d) Tabulated values of specific capacitance and MnO$_2$ normalized specific capacitance.[15]

EXPERIMENTAL TECHNIQUES AND METHODS

This section details the experimental techniques used to prepare the active material of the anodes of interest for subsequent study as well as the analytical techniques used to characterize these materials and the electrochemical testing done to assess their performance for LIB anode use. The chapter also gives an overview of the process of electrostatic spray deposition (ESD), the method chosen to deposit the active material as a thin film onto a substrate that would serve as the current collector for the LIB anodes.

3.1 Material Preparation

Preparation of the active material began with the acid treatment of multi-walled carbon nanotubes (MWCNTs) and subsequent filling with a precursor for the tin oxide. These procedures were based off those used by Chen *et al.* for a similar configuration that contained manganese oxide rather than tin oxide.[15] The MWCNTs were purchased from Cheap Tubes Inc., made via a chemical vapor deposition (CVD) process and purified by the vendor prior to sale. The outer diameters of the CNTs were 8-15 nm and the inner diameters were 3-5 nm. The purity was listed as >95% and the tubes were 10-50 μm in length. They had a specific surface area of 233 m^2/g, an electrical conductivity greater than 100 S/cm, a bulk density of 0.15 g/cm^3 and a true density of ~2.1 g/cm^3. For the desired nanoparticulate-filled MWCNTs to be produced, the CNTs first had to be treated with acid to open their ends, cut the tubes to a shorter length of ~0.2-1 μm, and remove any possible metal catalyst residue. The acid treatment was carried out in refluxing apparatus with a condenser tower attached to a round bottom flask containing the MWCNTs and sufficient

nitric acid (HNO_3, 70%) to completely cover and immerse the CNTs (~50 mL). The round bottom flask was immersed in a silicone oil bath to maintain even temperature distribution throughout the flask and the oil bath was raised to 140ºC and held at this temperature for 14 hours.

After the acid treatment of the CNTs was completed, the insertion of the tin oxide (SnO_2) nanoparticles had to be carried out to obtain the final active material for the desired LIB anodes. In order to obtain the SnO_2, tin (IV) acetate (Sigma Aldrich) was used as a precursor for subsequent oxidation to obtain the finished product. The tin (IV) acetate was dissolved in ethanol (50% w/w) and the acid treated CNTs were introduced to the mixture to obtain the desired weight ratio of SnO_2 to CNT (10%, 20%, 25%, or 30%) with stoichiometric calculations used to obtain the correct output of SnO_2 based on the quantity of tin (IV) acetate required. The weight fractions selected for this study were based on the values that would give a comparable molar ratio to those values used for the MnO_2 study by Chen *et al.*[15] The capillary forces of the CNTs were used to introduce the tin (IV) acetate precursor solution into the inner channels and the process was further aided with stirring and subsequent ultrasonic treatment for 2 hours. The resultant mixture was slowly dried at room temperature and the dried powder was heat-treated in air in a box furnace at 300ºC for four hours to allow oxidation of the tin (IV) acetate into SnO_2. Throughout this text, the samples prepared this way will be referred to as SnO_2-in-CNT. The control group samples that were used to compare confined vs. unconfined SnO_2 are denoted SnO_2-out-CNT.

3.2 Electrostatic Spray Deposition (ESD)

ESD is a thin film deposition method, originally detailed by J. Zeleny in 1914, which uses a voltage applied to the source of a solution and grounding of the substrate, on which the material is to be deposited, to atomize the solution via the applied field and draw it across a gap to create the final film.[22] Here, a precursor solution is loaded into a syringe and then a syringe pump is used to dispense the solution at a constant flow rate through a syringe needle to which the voltage source is connected. The substrate is heated to a sufficiently high temperature to allow the evaporation of the solvent. The applied field serves to charge the surface of the droplet that forms at the tip of the syringe needle that is typically used in this procedure and it is this charging that overcomes the surface tension and causes atomization. The advantages of using this technique are numerous. It is inexpensive, efficient, simple, does not need to be carried out under vacuum, and can be used to create a variety of different microstructures. This is made possible by the many parameters that can be adjusted for the deposition of a film. Film deposition parameters using ESD include: substrate temperature, applied voltage, precursor solution flow rate, deposition time, needle-to-substrate distance, and precursor solution composition. Fine tuning and optimizing these parameters can allow for the creation of many different microstructures of the films.[9,19–21] Figure 7 shows a schematic representation of the process of ESD and a photograph of the testing setup during use. The photograph shows the conical geometry of the atomized spray during thin film deposition.
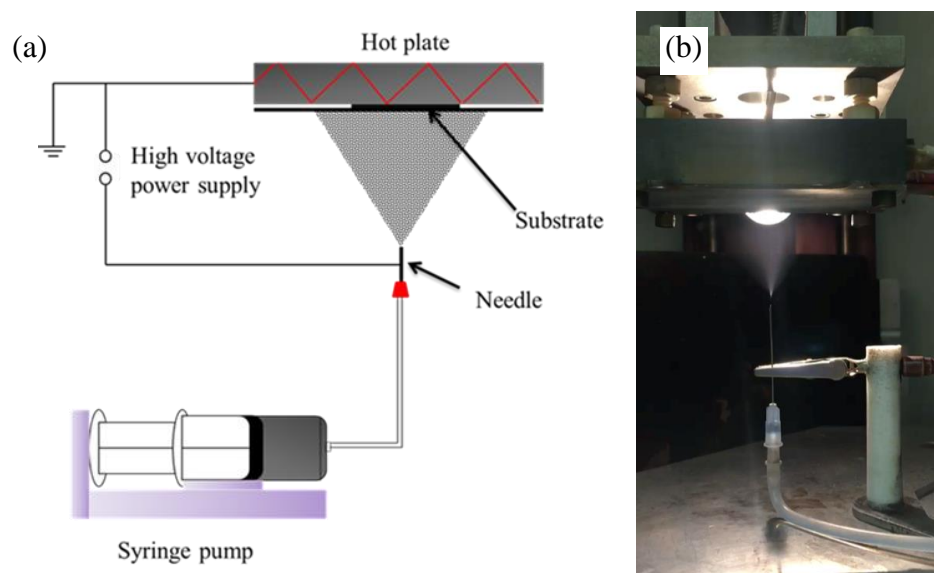
Figure 7: (a) Schematic representation of the ESD process and (b) photograph of setup.

The precursor solution used for ESD contained the SnO_2-in-CNT dissolved in a 60% ethanol, 40% 1,2 propanediol solvent mixture that was found to be the optimum for deposition of the active material of interest. Prior to use for ESD, the precursor solution was stirred and mixed ultrasonically for 1-2 hours until immediately prior to beginning ESD. For these tests, the parameters used for film deposition were a flow rate of ~4 mL/hour and a voltage of 5-8 kV. The substrate was always heated to 300ºC using a thermocouple to verify temperature. ESD is carried out in air at atmospheric pressure.

3.3 Structural and Morphological Characterization

In order to verify that the desired composition and structure of the active material of interest were obtained and that all the control groups were controlling for the correct parameters, several analytical techniques were used. The three main characterization methods used were x-ray diffraction (XRD), scanning electron microscopy (SEM), and

transmission electron microscopy (TEM), each of which served an important function in verification of the materials of interest.

3.3.1 X-Ray Diffraction (XRD)

X-ray diffraction is a technique that uses an incident x-ray beam to study the crystallographic structure of materials and identify material composition. For this work, XRD data was obtained using a Siemens D-5000 diffractometer with Cu Kα radiation (λ = 1.542 Å). Specifically, in this work this technique was used to assess the efficacy of the heat treatment in the experimental procedure in producing the desired SnO_2 in both the relevant control and experimental groups. Samples for XRD were collected as powder after deposition with ESD onto an aluminum plate without the nickel foam substrate.

3.3.2 Scanning Electron Microscopy (SEM)

To characterize the microstructure and morphology of the thin films deposited on our substrates via ESD, SEM was employed. SEM images were taken with a JEOL JSM-6330 field-emission scanning electron microscope (FESEM) working at 15.0 kV. The SEM is equipped with an energy dispersive x-ray spectrometer (EDS), which is used to identify the elemental composition of points or areas in an SEM image.

3.3.3 Transmission Electron Microscopy (TEM)

TEM is a powerful tool for gaining very high-resolution images of materials' microstructure and nanostructure, often even down to the level of atomic resolution for high resolution TEM (HRTEM). TEM imaging was carried out on a Phillips CM-200 200

kV Transmission Electron Microscope (TEM) with Energy Dispersive Spectroscopy (EDS). TEM was primarily used in this work to confirm confinement of SnO_2 within the MWCNTs and compare the control samples to the experimental samples to ensure that particles were unconfined in the SnO_2-out-CNT samples.

3.4 Assembly of Cells

For the anode material of interest to be properly tested electrochemically, half cells were assembled containing the deposited film on the nickel foam substrate with lithium metal serving as the lithium source for testing and cycling of the cells. Cell assembly was carried out in a glove box filled with argon gas and maintaining both the atmospheric oxygen and water levels at less than 1 ppm. The cells were assembled as coin cells in CR 2032 packaging. All half-cells contained a thin, permeable membrane polymer-based separator between the nickel foam substrate with active material and the lithium metal. All assembled cells used the same electrolyte, lithium hexafluorophosphate ($LiPF_6$, Sigma Aldrich, battery grade, $\geq$99% trace metals basis), for consistency and comparability of results.

3.5 Electrochemical Performance Testing

In order to compare the control and experimental group cells, various tests were carried out on the assembled half-cells. These tests include cyclic voltammetry (CV), galvanostatic charge-discharge testing, and rate capability testing. All electrochemical testing of the assembled coin cells was carried out after a delay of about 24-48 hours after cell assembly to give an adequate rest time for stabilization.

Cyclic voltammetry (CV) is useful to determine the reversibility of a reaction or reactions in the process of cycling an electrochemical cell or half-cell. It is carried out for a specified number of cycles within a fixed voltage window at a specified scan rate (mV/s) and measures the current response from electron transfer processes. Typically the first cycle differs most greatly from the subsequent cycles in any electrochemical test because of some irreversible capacity loss occurring after the first cycle. After this first cycle, most cells tend to stabilize. CV was carried out using a BioLogic VMP3 electrochemical testing setup. CV was carried out at rates of 0.1, 0.2, 0.5, 1.0, and 2.0 mVs^{-1}.

Galvanostatic charge-discharge tests are carried out by discharging and charging the half-cells for the desired number of cycles to determine overall trends in capacity retention, loss, or gain with use. A fixed current is chosen for charge and discharge of the cells and in this study discharging and charging were carried out for up to 200 cycles per half-cell. Rate capability testing operates similarly to the charge-discharge testing, but rather than test a half-cell for 100 cycles at one fixed current, different current values are tested for a number of cycles on a single cell to compare the capacity of the cell at different rates. All rate capability and charge-discharge tests were carried out on a Neware BTS-610 battery testing apparatus.

In order to determine the specific capacity of the active material of interest for all half-cells, masses were taken of the substrate before and after ESD was carried out to determine the mass deposited. That measured change in mass was used for all specific capacity calculations. All electrochemical testing was done on all half-cells at room temperature, ~25ºC.

3.6 Experiment Design and Controls

In order to accurately analyze the results of electrochemical performance obtained from testing the experimental group of interest, the study was designed to include necessary control groups for comparison. Specifically, this work hypothesized that the confinement of SnO_2 nanoparticles within the inner channels of MWCNTs would result in cells with improved electrochemical performance. This performance, therefore, had to be compared versus SnO_2 alone, MWCNTs alone, and unconfined SnO_2, referred to as SnO_2-out-CNT to differentiate from the confined samples. Therefore, SnO_2 samples were prepared by mixing the tin (IV) acetate precursor with closed MWCNTs, drying and heat treating via the same process detailed in section 3.1, and depositing this active material via ESD similarly onto a Ni foam substrate. Samples containing SnO_2 alone as the active material were prepared with ESD carried out using the tin (IV) acetate precursor dissolved in the same ratio combination of ethanol and 1,2 propanediol. The nickel foam substrate onto which the tin (IV) acetate was deposited was heated to 300ºC, above the oxidation temperature of 270ºC[17], and carried out in air. Full oxidation of tin (IV) acetate to SnO_2 was confirmed using XRD and the results are shown in Chapter IV.

CHAPTER IV

RESULTS AND DISCUSSION

4.1 Characterization Results

4.1.1 X-ray Diffraction (XRD)

X-ray diffraction was used in this study with the primary objective of verifying that the tin (IV) acetate that was used as a precursor material for the SnO_2 in both the control and experimental group samples had oxidized as expected to give the SnO_2. Therefore, for each group some powder was taken and XRD was carried out to identify the composition. Figure 8 shows the comparison of the XRD patterns for SnO_2 alone, SnO_2-in-CNT, SnO_2-out-CNT, and CNTs alone. The XRD results showed that the SnO_2 alone sample was indeed oxidized as desired from the tin (IV) acetate precursor, as were the experimental and control groups with SnO_2, thus validating the heat treatment step of the experimental procedure. that there was very little difference between the SnO_2-in-CNT and the SnO_2-out-CNT samples, as expected. The XRD pattern for the MWCNTs was typical and comparable to other XRD carried out on CNTs in prior literature.[23] The patterns show some overlap between the main CNT peak and the SnO_2 (110) peak. Additionally, the main contribution to the XRD patterns of the composite samples was the SnO_2, which can be attributed to the crystallinity of this material.
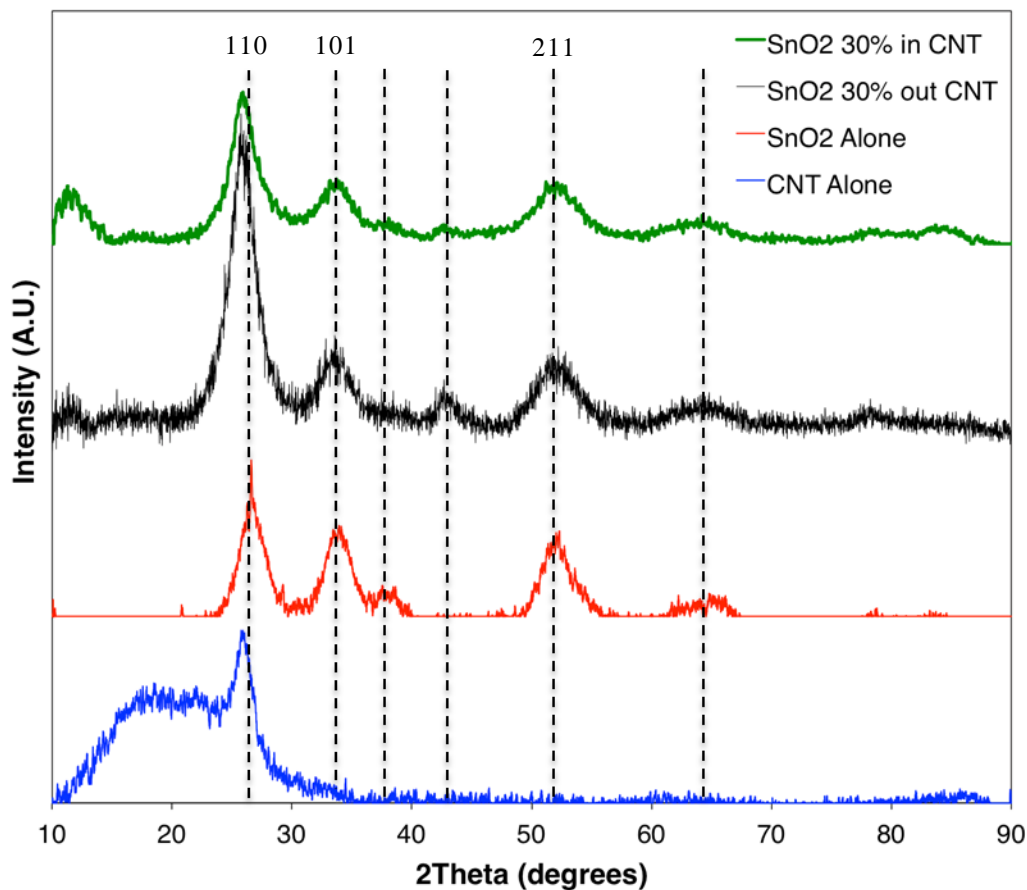
Figure 8: XRD data for confined, unconfined, SnO₂ alone, and CNT alone samples.

4.1.2 Scanning Electron Microscopy (SEM)

SEM was utilized to verify the microstructure of the deposited thin films onto the nickel foam current collector (substrate) to ensure that the deposited film was even and sufficiently porous to allow improved Li^+ ion diffusion into the active anode material. Figure 9 (a) shows an SEM image with 95x magnification where the larger structure of the porous nickel foam can be seen with an even thin film coating deposited on all visible surfaces. Figure 9 (b) at 550x magnification gives a more detailed image of one section of the nickel foam, highlighting both the porosity of the deposited film and its evenness at a 10 μm resolution. In Figure 9 (c), an enlarged view of the morphology is shown at a

magnification of 2,300x. The fourth SEM image, Figure 9 (d) was taken at 75,000x magnification, showing a representative region of the deposited film. In (d) individual CNTs are visible without any external agglomerated SnO_2, further supporting confinement of the SnO_2 particles within the CNTs.
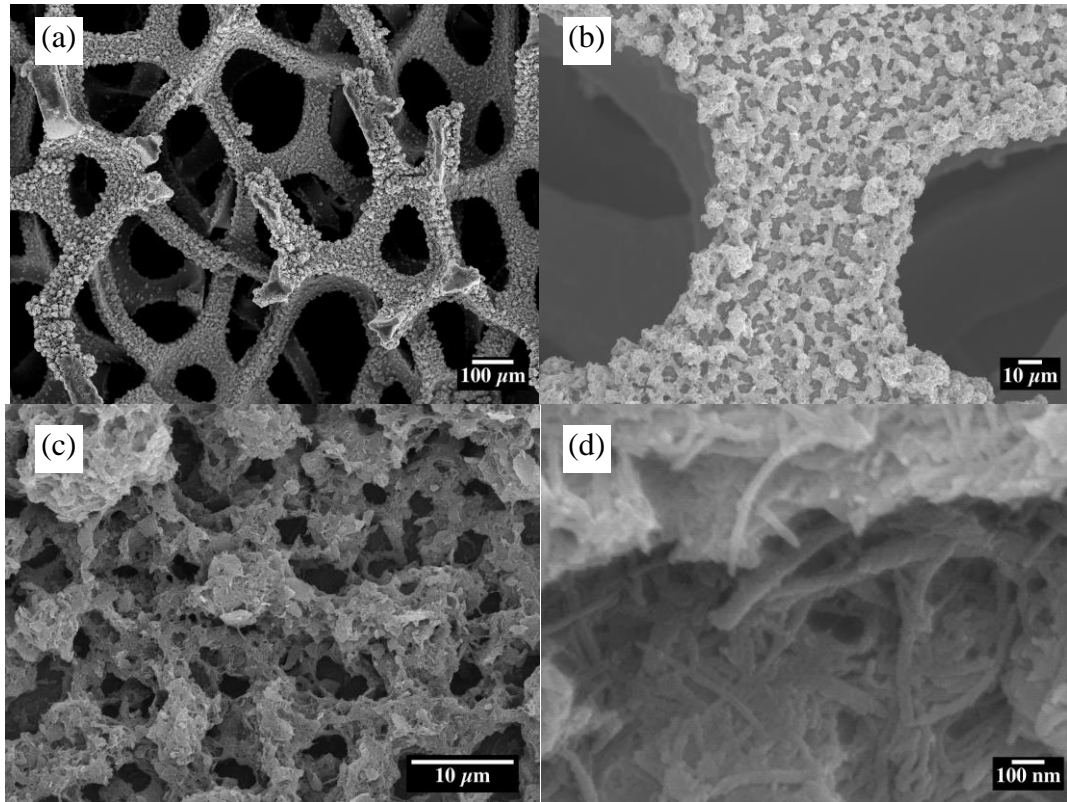
Figure 9: SEM of SnO_2-in-CNT sample with (a) 97x, (b) 550x, (c) 2,300x and (d) 75,000x magnifications

4.1.3 Transmission Electron Microscopy (TEM)

The purpose of TEM for this study was to confirm that confinement of SnO_2 within the CNTs was successfully achieved. Figure 10 shows TEM images of SnO_2-in-CNT sample where CNTs with SnO_2 nanoparticle are visible. In the TEM images, the MWCNTs were identified by the layered structure of the wall and the inner and outer diameter sizing being in keeping with the expected diameters from the manufacturer's specifications (8-15

nm outer diameter, 3-5 nm inner diameter. The SnO_2 nanoparticles are the darker spots within the CNTs visible in Figure 10. Figure 10 (a) and (b) show a magnified view of the individual carbon nanotube and SnO_2 particle with visible interplanar spacing. Figure 10 (c) shows the profile taken of the SnO_2 particle to confirm that the d-spacing was in-keeping with the predicted value for SnO_2, which was confirmed. Additional images with more carbon nanotubes and more SnO_2 particles, showing particulate confinement, are shown in (d) and (e).
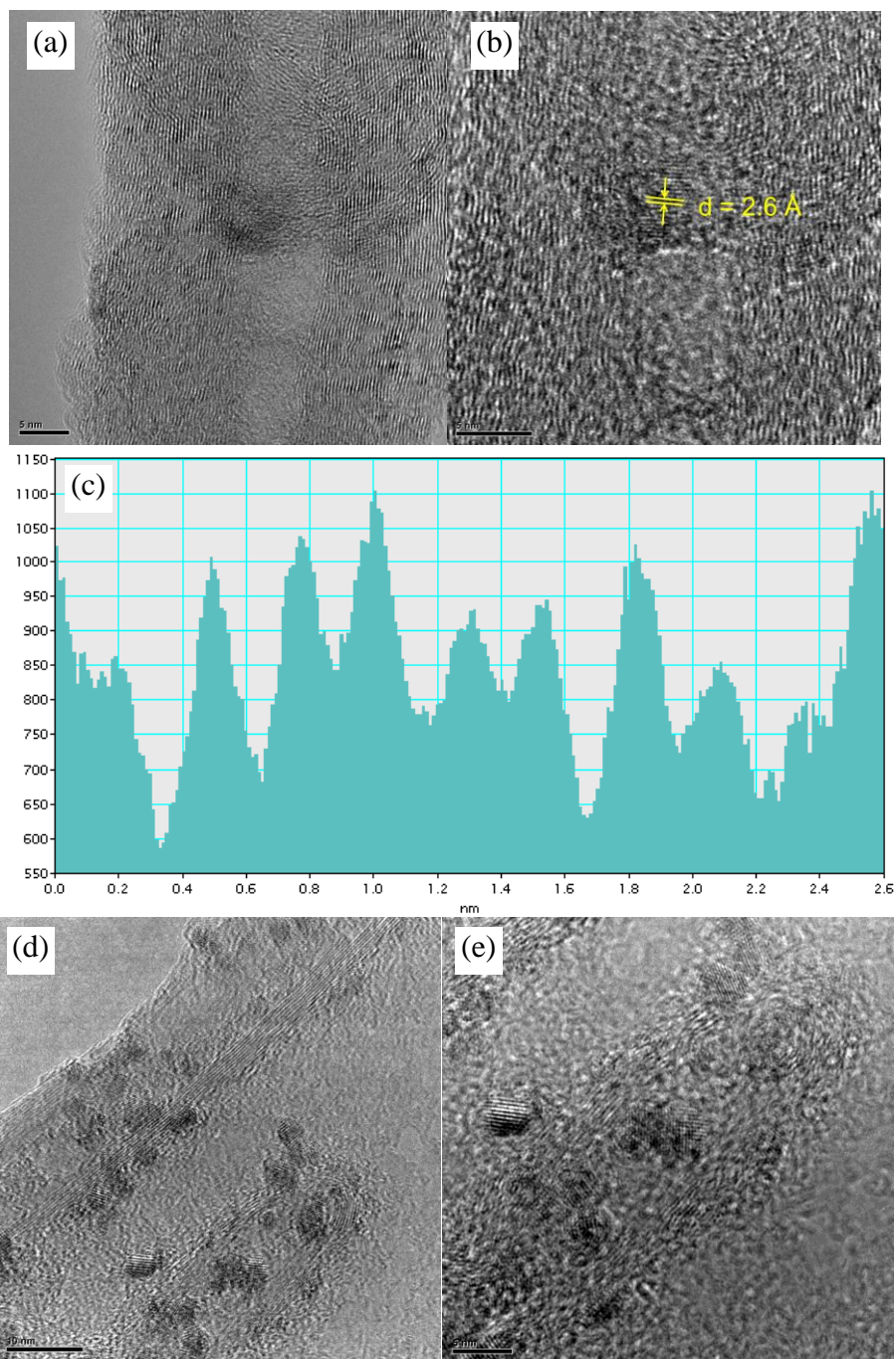
Figure 10: (a) and (b) TEM images showing an individual carbon nanotube, vertically oriented, with a tin oxide nanoparticle showing clear confinement with identification of the d-spacing between atomic planes (c) Profile of interplanar spacing for d = 2.6 Å corresponding to SnO_2. (d), and (e), showing confinement of SnO_2 particles within CNTs.

4.2 Electrochemical Results

In Figure 11 the results of cyclic voltammetry taken at a scan rate of 0.2 mVs-1 for the third cycle of the various sample groups are shown. For the tin oxide alone control sample, characteristic oxidation and reduction peaks are visible. The peak between 0.1 and 0.5 V corresponds to Li ions alloying with the metallic Sn that is a product of the first reaction step. The peak at ~1.0 V is attributed to the SEI formation and the peak at 1.35 V corresponds to the reduction of SnO2 to metallic Sn in the first reaction step. The reverse reaction is represented by the peak at about 1.2 V, which is visible in the SnO2 alone, and the 20% and 30% SnO2-in-CNT samples. Finally, the de-alloying process of Li leaving the Li_xSn compound is visible at about 0.55 V. The current response seen for CNTs alone was very small, as was that of the unconfined sample, which does not show the redox peaks as noticeably as the confined samples. Though the SnO_2 showed a large current response for the first few cycles, with subsequent cycles this response deteriorated greatly, resulting in high instability of the half-cell with cycling over time.
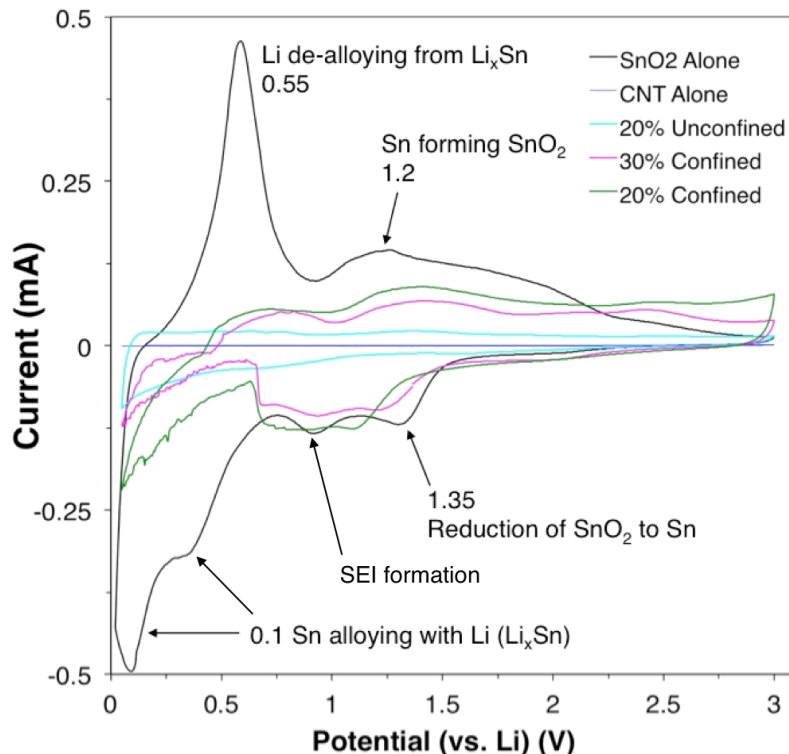
Figure 11: Cyclic voltammetry curves for experimental and control group samples

Figure 12 shows the galvanostatic charge-discharge curves for 20% SnO_2-in-CNT active material half-cell sample cycled at a rate of 100 mAg^{-1} through cycle 150 of discharging then charging the cell. With the first cycle, the cell shows the greatest value with the first discharge for specific capacity, with its maximum value falling at about 1300 mAhg^{-1}. For the discharge for cycle two, the specific capacity maximum fell at just under 700 mAhg^{-1}, about half the original value. This trend continues through cycle 10, however by cycle 40 the specific capacities steadily increased. In fact, the highest specific capacity measured on the charge side was seen with the charge step for cycle 150. The discharge cycles showed a gradual increase in the maximum measured specific capacity continuing through cycle 150 for which the value was greater than 900 mAhg^{-1}. Such trends are sometime seen in metal oxide anode materials and attributed to an electrochemical milling effect in which the particle size becomes reduced with cycling of the LIB.[24,25] A decrease

29

in the particle size then, consequently, results in an increased surface area of the metal oxide particles exposing a larger surface for reaction with Li^+ ions. This, in turn, is thought to be the cause of the gradual increase in specific capacity with cycling.
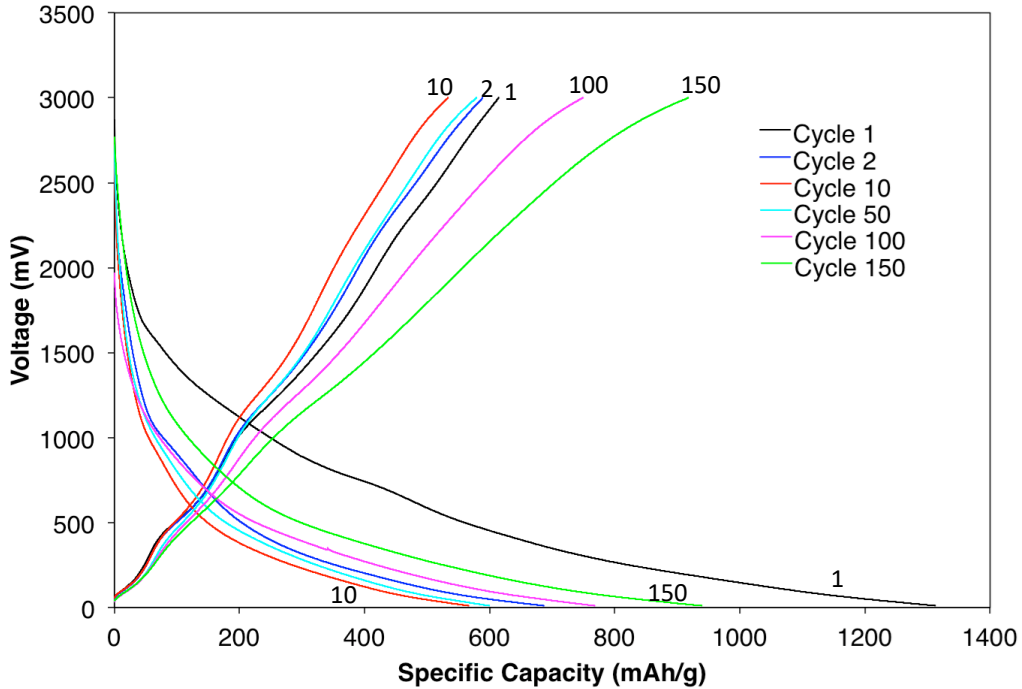

Figure 12: Galvanostatic charge-discharge curves for 20% SnO₂-in-CNT sample

A comparison of the cycle performances during discharge of the samples is presented in Figure 13 For the first 20 cycles, all of the samples showed a decreasing trend in specific capacities. By cycle 40, however, the confined samples (20, 25, and 30% SnO2-in-CNT) showed some recovery of capacity, a trend that continued through the hundredth cycle. The unconfined sample initially had good performance but continued decreasing in capacity with cycling and did not see the recovery achieved with the confined samples. This recovery of capacity can be attributed to an electrochemical milling process that is sometimes observed with cycling of LIB electrode materials[25] and also to the improved reversibility of the first reaction step of SnO_2 reacting with Li^+ ions to form metallic Sn

and Li_2O. In studies with nanoscale SnO_2 anodes, it was found that there was a greater reversibility of this first reaction step, giving a theoretical capacity of 1490 mAh/g.[10] With the electrochemical milling of SnO_2 and metallic Sn in the anode material, there could be a reduction of the particulate size and exposure of unreacted surfaces allowing for an improvement in the observed specific capacity. The CNT alone, as expected, had a low but stable value for specific capacity. Of the groups, the best capacity is observed with the 20% SnO_2-in-CNT sample. The values of specific capacity for the samples are tabulated in Table 3.
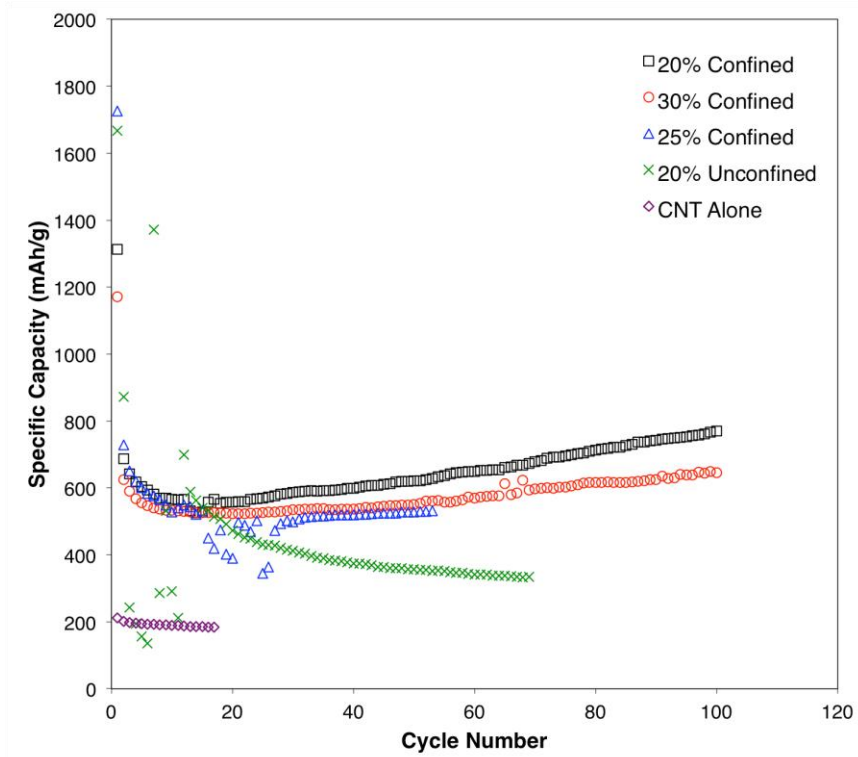

Figure 13: Cycle performances for the various control and experimental group samples

	Specific Capacity (mAh/g)					
	Cycle 1	Cycle 2	Cycle 10	Cycle 20	Cycle 40	Cycle 100
20% SnO_2-in-CNT	1312.3	686.5	566.3	558.3	599.4	770.6
25% SnO_2-in-CNT	1725.5	728.3	527.5	390.4	519.7	-
30% SnO_2-in-CNT	1170.4	625.3	533.3	523.5	537.2	645.9
20% SnO_2-**out**-CNT	1666.7	871.7	531.4	491.4	378.3	-
CNT Alone	211.2	201.6	190.4	183.5	-	-

Figure 14 shows the cyclic performance during discharge of the 20% SnO_2-in-CNT for 200 cycles with a testing rate of 100 mAhg^{-1} which very clearly shows the trend in initial specific capacity decrease for the first 15 cycles and subsequent increase for the remaining life of the cell through 200 cycles. The rate at which the specific capacity increased was fairly constant through cycle 100 and then increased slightly through cycle 200. The values of interest for the specific capacities at various cycle numbers were 1312.3, 686.5, 770.6, 943.1, and 1069.7 mAh/g at cycles 1, 2, 100, 150, and 200, respectively.
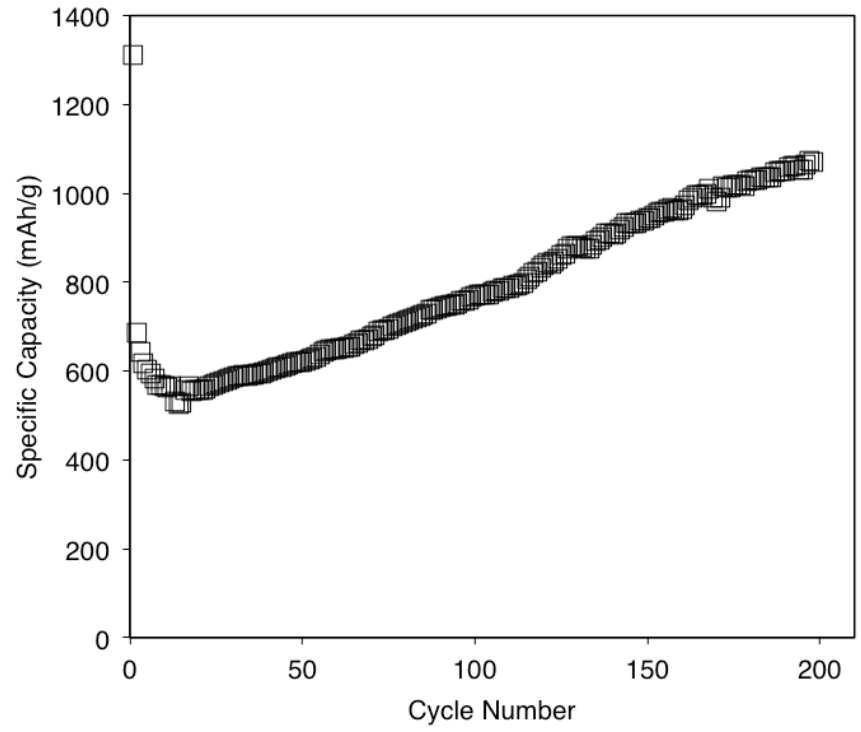
Figure 14: Cycle performance of 20% SnO$_2$-in-CNT for 200 cycles at 100 mAhg^{-1}

CHAPTER V

CONCLUSIONS

This thesis investigated the electrochemical performance and structural characteristics of composite lithium ion battery (LIB) anode materials containing SnO_2 nanoparticles confined within the inner channels of multiwalled carbon nanotubes. The technique used to deposit the active anode material onto a current collector (nickel foam substrate) was electrostatic spray deposition (ESD). The parameters for ESD were optimized to obtain films with the desired microstructure. Various SnO_2-to-CNT ratios were tested electrochemically (10%, 20%, 25%, and 30%) and the 20% SnO_2 confined within the CNT inner channels (denoted 20% SnO_2-in-CNT in this text) showed the most promising performance electrochemically. It was found with cycle performance testing that the specific capacity of the cells increased through 200 cycles with the 20% and 30% SnO_2-in-CNT samples, but with higher specific capacity for the 20% confined samples.

The third chapter of this manuscript detailed the experimental methods and techniques used to analyze the materials, including the optimized parameters for ESD for these materials and for the desired active material film morphology (porous). These parameters were a temperature of 300°C, a flow rate of ~4 mL/hour for the dispensing of the precursor solution from the syringe, and an applied voltage of 5-8 kV, adjusted to give the best spray of atomized solution (even, conical shape).

Chapter four detailed the results of the analytical methods, SEM, TEM, and XRD, and of the electrochemical tests that were carried out. XRD confirmed that the procedure used did give the desired output of SnO_2, which had been created via oxidation of a tin (IV)

acetate precursor. Additionally, there was overlap between the main CNT peak and the SnO$_2$ peaks and the main contribution to the XRD patterns of the SnO$_2$-in-CNT and SnO$_2$-out-CNT groups was the SnO$_2$. SEM was used to show that the films deposited had the desired morphology for electrochemical testing, showing an even, porous thin film material with good coating of the nickel foam substrate. TEM showed that there was confinement of the SnO$_2$ particles within the inner channel of the MWCNTs using the procedure detailed in chapter three. Finally, electrochemical testing was conducted for the various control and experimental groups and an interesting trend in initial capacity loss and eventual capacity recovery with cycling was observed for the SnO$_2$-in-CNT confined samples. This same recovery of capacity was not observed with the control group samples, and the best performance was observed with the 20% confined sample.

The future work recommended is to continue trying other weight ratios of SnO$_2$-in-CNT to determine the absolute optimum value. Additionally, the cycled batteries should be disassembled and TEM and SEM analysis carried out to analyze the microstructure, morphology, and nanostructure of the anodes after cycling. This would allow a better observation and understanding of the changes taking place during increased cycling to prove the reason for the observed increase in capacity. The anodes should also be paired with a commercially relevant cathode material and tested as a full cell to observe full cell performance. Finally, the structure tested for this composite material, with metal oxide confined within a CNT should be tested with other metal oxides or metals that could be improved by this structure.

LIST OF REFERENCES

1. J. Cabana, L. Monconduit, D. Larcher, and M. R. Palacín, *Adv. Mater.*, **22**, 170–192 (2010).

2. A. Abouimrane et al., *Nanotechnology for Lithium-Ion Batteries* Y. Abu-Lebdeh and I. Davidson, Editors, p. 1-362, Springer US, New York, NY, (2013) http://link.springer.com/10.1007/978-1-4614-4605-7.

3. M. Endo, C. Kim, K. Nishimura, T. Fujino, and K. Miyashita, *Carbon N. Y.*, **38**, 183–197 (2000).

4. H. Bin Wu, J. S. Chen, H. H. Hng, and X. W. D. Lou, *Nanoscale*, **4**, 2526–42 (2012) http://www.ncbi.nlm.nih.gov/pubmed/22460594.

5. G. Wu et al., *Appl. Surf. Sci.*, **315**, 400–406 (2014) http://dx.doi.org/10.1016/j.apsusc.2014.07.188.

6. G. Du et al., *Electrochim. Acta*, **55**, 2582–2586 (2010) http://linkinghub.elsevier.com/retrieve/pii/S0013468609015187.

7. L. Zou et al., *Carbon N. Y.*, **49**, 89–95 (2011) http://linkinghub.elsevier.com/retrieve/pii/S0008622310006226.

8. R. Agrawal, A. Nieto, H. Chen, M. Mora, and A. Agarwal, *ACS Appl. Mater. Interfaces*, **5**, 12052–7 (2013) http://www.ncbi.nlm.nih.gov/pubmed/24236402.

9. C. Chen et al., *ECS Trans.*, **61**, 155–163 (2014).

10. J. Guo, B. Jiang, X. Zhang, and H. Liu, *J. Power Sources*, **262**, 15–22 (2014) http://dx.doi.org/10.1016/j.jpowsour.2014.03.085.

11. A. Dhanabalan, X. Li, R. Agrawal, C. Chen, and C. Wang, *Nanomaterials*, **3**, 606–614 (2013) http://www.mdpi.com/2079-4991/3/4/606/.

12. C. Chen, R. Agrawal, and C. Wang, in *Proc. of SPIE*, N. K. Dhar and A. K. Dutta, Editors, vol. 9865, p. 986507 (2016) http://proceedings.spiedigitallibrary.org/proceeding.aspx?doi=10.1117/12.2228905.

13. C. Chen, R. Agrawal, Y. Hao, and C. Wang, *ESC Solid State Sci. Technol.*, **2**, 3074–3077 (2013).

14. C. K. Chan et al., *Nat. Nanotechnol.*, **3**, 31–35 (2008) http://www.nature.com/doifinder/10.1038/nnano.2007.411.

15. W. Chen, Z. Fan, L. Gu, X. Bao, and C. Wang, *Chem. Commun. (Camb).*, **46**, 3905–3907 (2010).

16. Y. Yu et al., *Angew. Chemie Int. Ed.*, **48**, 6485–6489 (2009) http://doi.wiley.com/10.1002/anie.200901723.

17. X. Li, A. Dhanabalan, L. Gu, and C. Wang, *Adv. Energy Mater.*, **2**, 238–244 (2012) http://doi.wiley.com/10.1002/aenm.201100380.

18. J. Chmiola et al., *Science (80-.).*, **313**, 1760–1763 (2006).

19. C. Chen, R. Agrawal, and C. Wang, **9865**, 986507 (2016) http://proceedings.spiedigitallibrary.org/proceeding.aspx?doi=10.1117/12.2228905.

20. R. Agrawal, C. Chen, and C. Wang, in *Proc. of SPIE*, N. K. Dhar and A. K. Dutta, Editors, vol. 9865, p. 986508 (2016) http://proceedings.spiedigitallibrary.org/proceeding.aspx?doi=10.1117/12.2228899.

21. Y. Yu, Y. Shi, C. H. Chen, and C. L. Wang, *J. Phys. Chem. C*, **112**, 4176–4179 (2008).

22. J. Zeleny, *Phys. Rev.*, **3**, 69–91 (1914).

23. A. Cao, C. Xu, J. Liang, D. Wu, and B. Wei, *Chem. Phys. Lett.*, **344**, 13–17 (2001).

24. Y. Yu, Y. Shi, and C.-H. Chen, *Nanotechnology*, **18**, 55706 (2007) http://stacks.iop.org/0957-4484/18/i=5/a=055706?key=crossref.47ff47cbbe3ad4a45533f4eb361e9cf4.

25. D. W. Zhang, C. H. Chen, J. Zhang, and F. Ren, *Chem. Mater.*, **17**, 5242–5245 (2005).